MODELLING THE EFFECT OF FORCED UNSTEADINESS ON FLOW AND HEAT TRANSFER IN SEPARATED AND REATTACHING FLOWS

Tim Craft, Hector Iacovides, Parham Momeni
School of Mechanical, Aerospace and Civil Engineering,
The University of Manchester
M60 1QD, United Kingdom
Email: P.Momeni@Postgrad.manchester.ac.uk

ABSTRACT

The present paper describes the numerical modelling of turbulent flow and convective heat transfer for two types of two-dimensional forced unsteady flows: periodically oscillating flow through an abrupt pipe expansion, and flow over a backward facing step with periodic injection and ingestion through a slot at the separation corner. In both cases the flow Reynolds numbers are reasonably high and emphasis is placed on the resulting heat transfer rates in the separated and recovery regions of the flow.

The present work tests the two-equation linear $k-\varepsilon$ (Launder and Sharma, 1974) and a modified two-equation non-linear $k-\varepsilon$ (Craft et al., 2005) turbulence model in conjunction with the Reynolds-averaged momentum (URANS) and temperature equations. The imposed unsteadiness enhances the coherence of the separated shear layers and reduces the reattachment lengths. Both models are shown to broadly capture this effect, with the non-linear scheme giving better quantitative agreement with available experimental data.

Key words: Eddy-viscosity model, Convective heat transfer, Imposed unsteadiness, URANS.

INTRODUCTION

Flows involving separation and reattachment are found in a very wide range of engineering systems. In heating or cooling applications, heat transfer rates between the fluid and surrounding walls typically show maximum levels around reattachment points, and a popular method of increasing heat transfer rates is thus to mount roughness elements onto walls, resulting in separation and the associated turbulent mixing.

Many flows involving large separated regions, particularly those associated with flow around bluff bodies, tend to exhibit large-scale unsteadiness. However, another important form of time-dependence, which is the subject of this investigation, is the response of the flow to imposed unsteadiness, which can have a significant influence on the performance of many thermal engineering applications such as refrigerating systems, reciprocating compressors, internal combustion engines, and pulsing combustion systems. In particular, we focus here on the effect of such forcing on the flow patterns and heat transfer rates in separated flows.

There are considerable modelling challenges in computing flows exhibiting even steady separation and reattachment. Furthermore, to minimize computing times – particularly important in unsteady flows, given the requirement to perform a large number of time steps – there is a desire to employ relatively simple RANS models of turbulence. However, simple linear eddy-viscosity models are known to perform badly in steady separated flows, and even non-linear eddy-viscosity models do not all produce accurate and reliable results.

In a recent study, Craft et al (2005) introduced refinements to a non-linear eddy-viscosity model and showed that this performed quite successfully in predicting the steady flow and heat transfer through a sudden pipe expansion over a range of Reynolds numbers. The present study aims to test the performance of this scheme in computing unsteady separated flows.

In the present study two flow geometries are considered: flow over a backward facing step with periodic injection and ingestion through a slot at the separation corner, and periodically oscillating flow through an abrupt pipe expansion. One effect of the imposed unsteadiness is to reduce the averaged reattachment length, which subsequently affects the heat transfer performance, although the magnitude of these effects is strongly dependant on the frequency of the perturbations.

The following sections outline the modelling approaches tested, describe the flow cases considered, and present comparisons between the model predictions and available experimental data.

MODELLING APPROACH

Two-Equation Linear $k-\varepsilon$ Model:

The simplest model employed in this study is the linear $k-\varepsilon$ scheme of Launder & Sharma (1974), which approximates the turbulent stresses and heat fluxes by

$$\overline{u_i u_j} = \frac{2}{3} k\ \delta_{ij} - \nu_t \left(\frac{\partial U_i}{\partial x_j} + \frac{\partial U_j}{\partial x_i} \right) \tag{1}$$

$$\overline{u_j t} = -\frac{\nu_t}{\sigma_t} \frac{\partial T}{\partial x_j} \tag{2}$$

where the turbulent viscosity $\nu_t = c_\mu\ f_\mu\ k^2 / \tilde{\varepsilon}$ and k and $\tilde{\varepsilon}$ are obtained from the transport equations

$$\frac{D(k)}{Dt} = \frac{\partial}{\partial x_j}\left(\left(v + \frac{v_t}{\sigma_k}\right)\frac{\partial k}{\partial x_j}\right) + P_k - \varepsilon \quad (3)$$

$$\frac{D(\tilde{\varepsilon})}{Dt} = \frac{\partial}{\partial x_j}\left(\left(v + \frac{v_t}{\sigma_{\tilde{\varepsilon}}}\right)\frac{\partial \tilde{\varepsilon}}{\partial x_j}\right) + C_{\varepsilon 1} f_1 \frac{P_k \tilde{\varepsilon}}{k} - C_{\varepsilon 2} f_2 \frac{\tilde{\varepsilon}^2}{k} + E + Y_{dc} \quad (4)$$

where $\varepsilon = \tilde{\varepsilon} + 2v\left(\frac{\partial k^{0.5}}{\partial x_j}\right)^2$.

The production rate of turbulent kinetic energy, P_k, is given by

$$P_k = -\overline{u_i u_j}\frac{\partial U_i}{\partial x_j} \quad (5)$$

whilst E is the near-wall source term

$$E = 2\, v\, v_t \left(\frac{\partial^2 U_i}{\partial x_j \partial x_k}\right)^2 \quad (6)$$

The term Y_{dc} is the lengthscale correction originally proposed by Raisee (1999), and subsequently re-tuned by Craft et al. (2005), which is based on lengthscale gradients, and can be written as

$$Y_{dc} = C_w \frac{\tilde{\varepsilon}^2}{k}\max\left[F^{0.4}(F+1)^2, 0\right] \quad (7)$$

where F essentially measures the difference between the predicted lengthscale gradient and the value it would take in an equilibrium boundary layer:

$$F = \frac{1}{C_l}\left\{\left[\left(\frac{\partial l}{\partial x_j}\right)\left(\frac{\partial l}{\partial x_j}\right)\right]^{0.5} - dl_e / dy\right\} \quad (8)$$

with $l = (k^{1.5}/\varepsilon)$ and the term dl_e/dy standing for the equilibrium lengthscale gradient, given by:

$$C_l[1 - \exp(-B_\varepsilon \tilde{R}_t)] + B_\varepsilon C_l \tilde{R}_t \exp(-B_\varepsilon \tilde{R}_t) \quad (9)$$

The various model coefficients and near-wall damping terms are given in Table 1, whilst $\tilde{R}_t$ is the turbulent Reynolds number, $\tilde{R}_t = k^2/(\tilde{\varepsilon}\, v)$.

Table 1: Coefficients and damping functions in the linear $k-\varepsilon$ model

σ_k , $\sigma_{\tilde{\varepsilon}}$, σ_t f_1 , f_2	1 , 1.3 , 0.9 1 , $1-0.3\exp\left(-\tilde{R}_t^{\,2}\right)$
c_μ , f_μ	0.09 , $\exp\left(\frac{-3.4}{(1+\tilde{R}_t/50)^2}\right)$
C_l, B_ε, C_w	2.55 , 0.1069 , 083
$C_{\varepsilon 1}, C_{\varepsilon 2}$	1.44 , 1.92

Two-Equation Non-Linear $k-\varepsilon$ Model:

The above linear EVM is known to have many weaknesses, so much of the present model testing has been carried out within the framework of non-linear eddy-viscosity models. The first form tested is that proposed by Craft et al. (1996), which was itself a development of the cubic non-linear EVM of Suga (1996). In this scheme, the Reynolds stresses are approximated by

$$\begin{aligned}\overline{u_i u_j} = {} & (2/3)\, k\delta_{ij} - v_t S_{ij} \\ & + C_1 \frac{v_t}{\tilde{\varepsilon}} k\left(S_{ik}S_{jk} - (1/3)\, S_{kl}S_{kl}\delta_{ij}\right) \\ & + C_2 \frac{v_t}{\tilde{\varepsilon}} k\left(\Omega_{ik}S_{jk} + \Omega_{jk}S_{ik}\right) \\ & + C_3 \frac{v_t}{\tilde{\varepsilon}} k\left(\Omega_{ik}\Omega_{jk} - (1/3)\Omega_{kl}\Omega_{kl}\delta_{ij}\right) \\ & + C_4 \frac{v_t k^2}{\tilde{\varepsilon}^2}\left(S_{ki}\Omega_{lj} + S_{kj}\Omega_{li}\right)S_{kl} \\ & + C_6 \frac{v_t k^2}{\tilde{\varepsilon}^2}\left(S_{ij}S_{kl}S_{kl}\right) + C_7 \frac{v_t k^2}{\tilde{\varepsilon}^2}\left(S_{ij}\Omega_{kl}\Omega_{kl}\right)\end{aligned} \quad (10)$$

where S_{ij} and Ω_{ij} are the strain and vorticity tensors, defined as

$$S_{ij} = \left(\frac{\partial U_i}{\partial x_j} + \frac{\partial U_j}{\partial x_i}\right), \quad \Omega_{ij} = \left(\frac{\partial U_i}{\partial x_j} - \frac{\partial U_j}{\partial x_i}\right) \quad (11)$$

In modelling the turbulent eddy viscosity, the quantities f_μ and c_μ are taken as

$$f_\mu = f_{\mu i} f_s + (1 - f_s) \quad (12)$$

with

$$f_{\mu i} = 1 - \exp\left(-\left(\tilde{R}_t/90\right)^{0.5} - \left(\tilde{R}_t/400\right)^2\right) \quad (13)$$

$$f_s = \min\left(\frac{\max\left((P_k/\tilde{\varepsilon})\min\left(1, \tilde{R}_t/50\right)^2, 0\right)}{0.75}, 1\right) \quad (14)$$

and

$$c_\mu = \min\left[0.09, \frac{1.2}{1 + \alpha\,\eta + f_{RS}}\right] \quad (15)$$

with

$$\alpha = 3.5 - 0.5\left(1 - \exp\left(-\left(\frac{\tilde{R}_t}{400}\right)^2\right)\right) \quad (16)$$

where

$$\eta = \max(\tilde{S}, \tilde{\Omega}) \quad (17)$$

and

$$f_{RS} = 0.235\left[\max(0, \eta - 3.333)\right]^2 \exp(-\tilde{R}_t/400) \quad (18)$$

$$\tilde{S} = \frac{k}{\tilde{\varepsilon}}\sqrt{\frac{(S_{ij}S_{ij})}{2}}, \quad \tilde{\Omega} = \frac{k}{\tilde{\varepsilon}}\sqrt{\frac{(\Omega_{ij}\Omega_{ij})}{2}} \quad (19)$$

The remaining model coefficients are given in Table 2.

Table 2 : Coefficients in the two-equation cubic stress-strain relation

C_1	C_2	C_3	C_4	C_6	C_7
-0.1	0.1	0.26	$-10\,c_\mu^2$	$-5\,c_\mu^2$	$5\,c_\mu^2$

The $\tilde{\varepsilon}$ equation is similar to that employed in the Launder-Sharma model, but the near-wall source term E is replaced by

$$E=\begin{cases}0.0022\dfrac{\nu_t \tilde{S} k^2}{\tilde{\varepsilon}}\left(\dfrac{\partial^2 U_i}{\partial x_j \partial x_k}\right)^2 & \tilde{R}_t \le 250 \\ 0 & \tilde{R}_t > 250\end{cases} \tag{20}$$

and the coefficient employed in the lengthscale correction Y_{dc} in equation (7) is modified as

$$\begin{aligned}C_w=&\frac{\left\{3.4\,(1-f_s)\left(\min\,(1,\tilde{R}_t/25)\right)^2\right\}}{[0.8+0.7\,(\eta'/3.33)^4\exp(-\tilde{R}_t/12.5)]}\\&+\frac{\left\{0.75\,f_s\,\min\,(1,\tilde{R}_t/40)\right\}}{[0.8+0.7\,(\eta'/3.33)^4\exp(-\tilde{R}_t/12.5)]}\end{aligned} \tag{21}$$

where the quantity η' is defined as $\eta'=\max\,(\tilde{S}',\tilde{\Omega}')$ and $\tilde{S}'$ and $\tilde{\Omega}'$, are taken as

$$\begin{aligned}\tilde{S}'&=\left(\max\left[\frac{k}{\tilde{\varepsilon}},\sqrt{\frac{\nu}{\tilde{\varepsilon}}}\right]\right)\sqrt{\frac{1}{2}S_{ij}S_{ij}}\\ \tilde{\Omega}'&=\left(\max\left[\frac{k}{\tilde{\varepsilon}},\sqrt{\frac{\nu}{\tilde{\varepsilon}}}\right]\right)\sqrt{\frac{1}{2}\Omega_{ij}\Omega_{ij}}\end{aligned} \tag{22}$$

CASES STUDIED

The first case to be examined is that studied experimentally by Chun & Sung (1996), as shown in Figure 1, consisting of flow over a backward facing step, which is subjected to a periodic forcing via a small slot at the step corner.

The inlet conditions are a partially developed channel flow which is calculated in a separate simulation to match the experimental data just before the step. For the thermal field, a constant heat flux is imposed on the bottom wall, and the top wall is treated as adiabatic. The local forcing arises from a slot jet at the step corner, where the width of the slot is *0.02H* (*H* being the step height). The jet velocity here is assumed to have a uniform spatial profile, but varies sinusoidally in time as

$$U_j(t)=A\,U_0\sin(2\pi f t) \tag{23}$$

where A is defined as the forcing amplitude. The predictions were carried out for a bulk inlet Reynolds number of 33000, over a range of frequencies, $0 < St_H < 1$ (where the Strouhal number $St_H = fH/U_o$), and at two forcing amplitudes of $A = 0.03$ and 0.07.

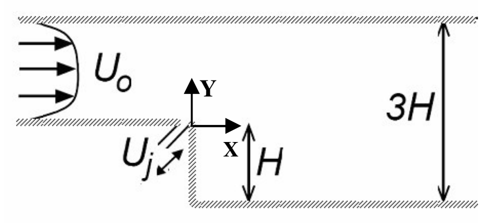

Figure 1 : Geometry of the flow studied experimentally by Chun & Sung (1996).

The second case considered is flow through a pipe expansion with geometry as shown in Figure 2, where H represents the height of the expansion, and the downstream to upstream radius ratio is 2.5.

The oscillating flow through this expansion is driven by imposing a time-dependent inlet velocity upstream of the expansion. These inlet conditions were obtained by running separate simulations of flow through a long pipe section, imposing a time-varying mass flow rate of the form

$$\dot{m}_{in}=\dot{m}_{\text{average}}\,(1+A\sin(2\pi\, f\, t)) \tag{24}$$

with $\dot{m}_{\text{average}}$ corresponding to the average bulk Reynolds number. The fully developed time-dependent flow profiles from these calculations were then imposed as inlet conditions for the pipe expansion case. Zero gradients in the axial direction were imposed at the exit, and a constant heat flux applied along the wall in the expanded section of the pipe.

The average Reynolds number (based on downstream averaged bulk velocity and downstream pipe diameter) was 40000, and a range of oscillation amplitudes, A ($0.05<A<0.5$), and Strouhal numbers ($0.03 < St_H < 3$) have been examined.

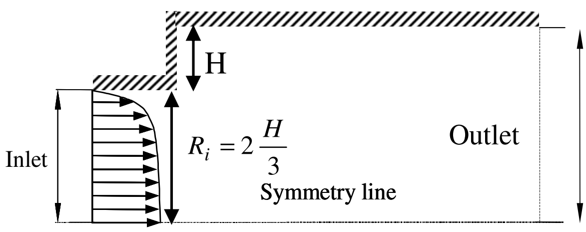

Figure 2 : Geometry of the pipe-expansion case studied by Yap (1987).

NUMERICAL IMPLEMENTATION

The computations have been performed using an in-house FORTRAN code, based on the finite-volume scheme with a semi-staggered grid arrangement. The pressure-velocity coupling is handled by the SIMPLE scheme, and the bounded QUICK scheme of Iacovides (1999) is used for approximation of convection. In order to prevent stability problems associated with pressure-velocity decoupling, a form of the Rhie & Chow (1983) interpolation scheme, suitable for a semi-staggered mesh, is also adopted.

Since low-Reynolds-number models are used in the present study, the grid must be fine enough to capture the steep gradients that occur near the wall. A strong separated shear layer is also expected away from the wall, so a reasonably fine grid is needed there also.

The Crank-Nicolson scheme has been used in all the unsteady computations. Grid and time sensitivity tests were performed using different grid densities and time steps, and these showed that the results presented for both cases can be considered essentially grid and time-step independent.

RESULTS

Case 1: Backward Facing Step

As noted above, one of the effects of the imposed forcing is to reduce the length of the time-averaged separation zone. Chun and Sung (1996) performed measurements over a range of Strouhal numbers, and reported that the maximum effect was achieved at a Strouhal number of 0.275, close to the natural shedding frequency of the separated shear layer. The first set of calculations has therefore been conducted with a forcing amplitude (*A*) of 0.07 and a Strouhal number of 0.275.

Figure 3 shows the computed time-averaged streamlines, using the non-linear $k-\varepsilon$ model, together with those predicted by the same model for the equivalent case without local forcing. The predicted reduction in reattachment length can clearly be seen, with reattachment occurring at around *X/H=5.5* for the forced case compared with *X/H=7.5* in the unforced flow. This reduction in the recirculation length is further underlined by Figure 4 which shows the measured and predicted time-averaged C_p values along the bottom wall (where $C_p = 0.5(P-P_0)/(\rho U_0^2)$ and P_0 is the reference value of the static pressure at *X/H=-2*). The rapid increase in C_p, associated with reattachment, can be seen to be more abrupt, and to occur further upstream, in the forced case compared to the steady state flow, corresponding to a smaller separation zone. Whilst both models predict a decrease in the reattachment length, the non-linear model is seen to give a better quantitative description of the C_p distribution in both the steady and forced cases.

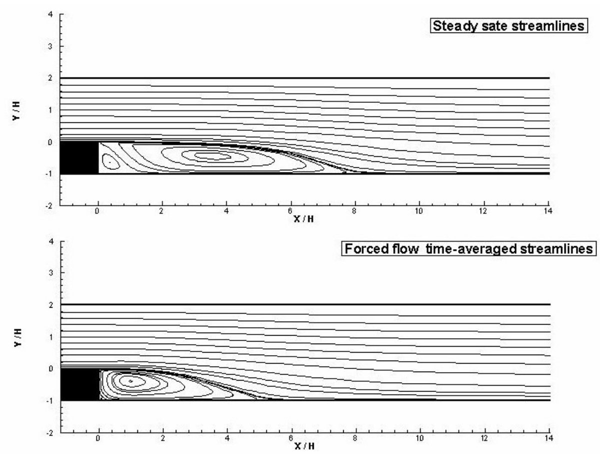

Figure 3 : Steady and forced flow time-averaged streamlines with non-linear $k-\varepsilon$ model.

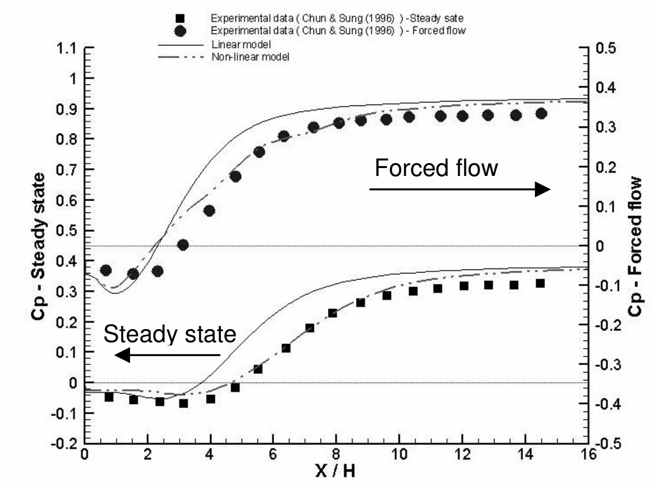

Figure 4 : Pressure coefficient along the upper channel wall with linear and non-linear $k-\varepsilon$ models.
Upper graph: Time averaged values in forced flow;
Lower graph steady state flow.

Streamwise velocity profiles, at a selection of positions, for the steady case, and corresponding time-averaged profiles for the forced case are shown in Figure 5. Again, the reduced reattachment length can clearly be seen in the unsteady forced case. Both models return stronger back-flow velocities within the separated region in the forced case (see profiles at *X/H=1*), implying a smaller, but more intense, recirculation zone. In general both models show reasonable agreement with the data in the separated shear region, although the recovery after reattachment is predicted to occur a little too slowly.

Corresponding profiles of the streamwise normal stress, $\overline{u^2}/U_0^2$, are shown in Figure 6. Here it can be seen that both models do capture the higher levels of turbulence measured in the unsteady case than the steady case for *X/H <5*, and are in broad agreement with the experimental data elsewhere, although the non-linear model tends to return slightly too high levels of normal stress, and shows some unphysical 'spikes' in the highly unsteady region of the separated shear layer. Further downstream the changes in the turbulent energy levels formed by the local forcing are observed to diminish.

As noted earlier, the magnitude of the reduction in the recirculation length is dependent on the forcing frequency. Figure 7 shows predicted and measured reattachment lengths (normalised with that of the steady case) for an amplitude of *A=0.03* over a range of Strouhal numbers. Both models broadly reproduce the measured features, with the forcing having a maximum effect at a Strouhal number of around 0.275, although the non-linear scheme clearly gives a much better quantitative reduction of the reattachment length. At higher frequencies ($St_H > 0.6$), both models tend to overpredict the effect the forcing has on the time-averaged reattachment length.

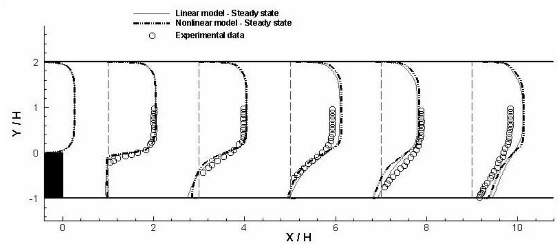

a) Steady state

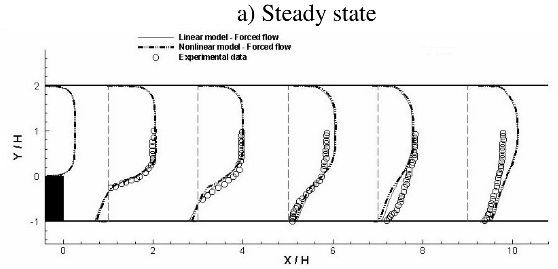

b) Forced flow

Figure 5 : Time-averaged non-dimensional velocity (U / U_0) profiles with linear and non-linear $k-\varepsilon$ models.

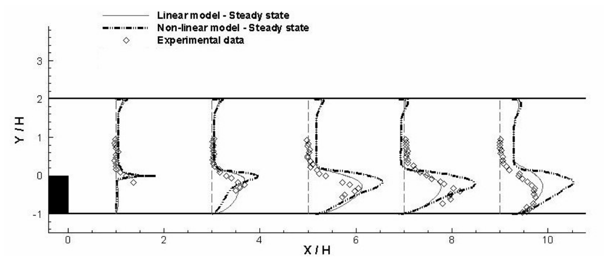

a) Steady state

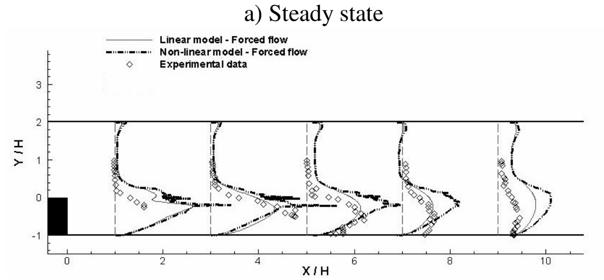

b) Forced flow

Figure 6 : Time-averaged non-dimensional normal-stress ($\overline{u^2} / U_0^2$) profiles with linear and non-linear $k-\varepsilon$ models.

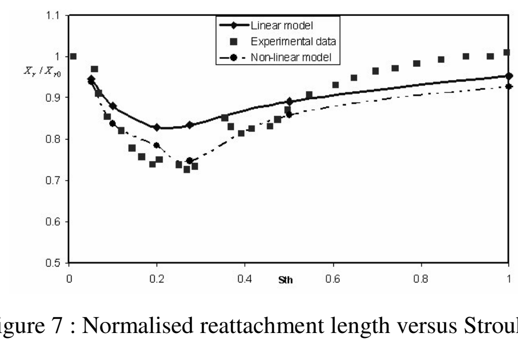

Figure 7 : Normalised reattachment length versus Strouhal number with linear and non-linear $k-\varepsilon$ models.

Case 2: Pipe Expansion

In the second case studied, a range of oscillation amplitudes, A, and Strouhal numbers (fH / U_o) have been examined. ($A = 0.1, 0.2, 0.5$) , ($St_H = 0.03, 0.075, 0.15, 0.3, 0.75, 1.5, 3$). Predicted results of the time-averaged reattachment length, X_r, (normalised with its steady state value X_{r0}) are presented in Figure 8 as a function of the non-dimensional forcing frequency. The forcing is seen to produce a qualitatively similar decrease in reattachment length to that noted in the step case, with a maximum reduction occurring at a Strouhal number of around 0.3. However, the magnitude of the maximum reduction is somewhat less in this case.

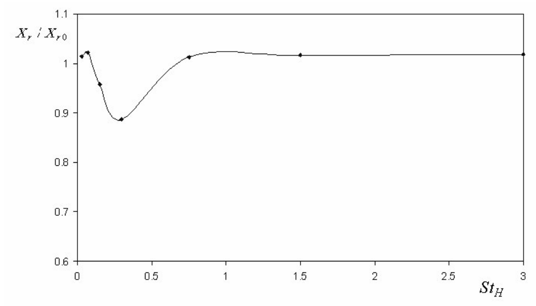

Figure 8 : Normalised reattachment length versus Strouhal number with non-linear $k-\varepsilon$ model.

Further understanding of the unsteady case can be gained from examining the phase-averaged flow field at different times through the cycle. Predicted phase averaged streamlines at $St_H = 0.3$ and $A = 0.2$ are shown in Figure 9, demonstrating the highly unsteady response of the separation pattern to the imposed forcing. The interaction of the vortices as they roll up, coalescence and separate produces the higher levels of turbulence referred to earlier, and the shorter time-averaged separation zone.

Figure 10 shows the time averaged Nusselt number distribution for the case with $A = 0.2$ and Strouhal number of 0.4. Also shown are the predicted values for the steady flow at the same average Reynolds number, which can be seen to be in good agreement with the measured data of Yap (1987). In the forced case the predicted maximum Nusselt number value is slightly lower, and occurs slightly further upstream, than that in the steady case. However, in the near-corner region ($X/H < 4$) the unsteady flow case returns significantly higher average values of heat transfer. The reasons for these differences are again related to the effects of forcing on the reattachment length. The forcing results in a shorter, but more intense, separated flow region, leading to the illustrated changes in heat transfer levels.

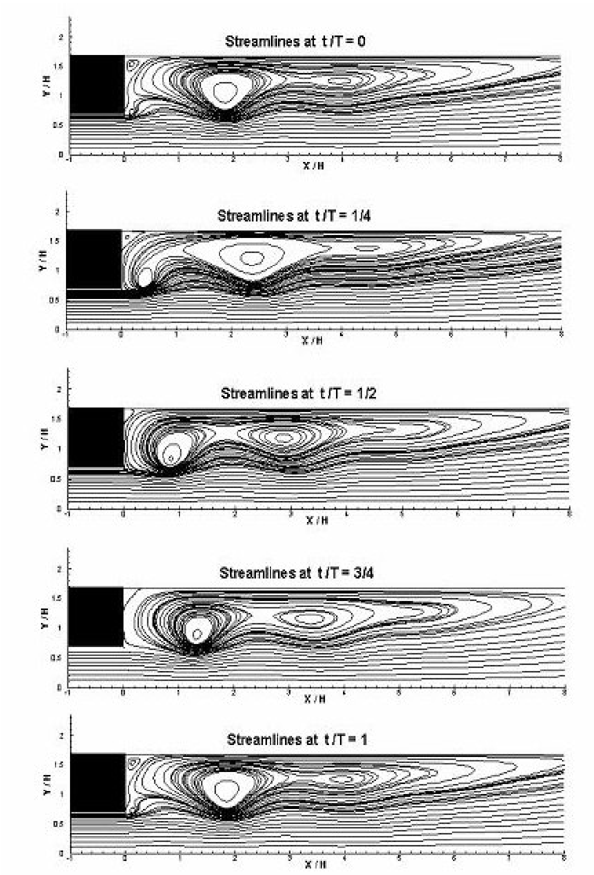

Figure 9 : Predicted phase averaged streamlines of flow through the pipe expansion at selected times through the cycle.

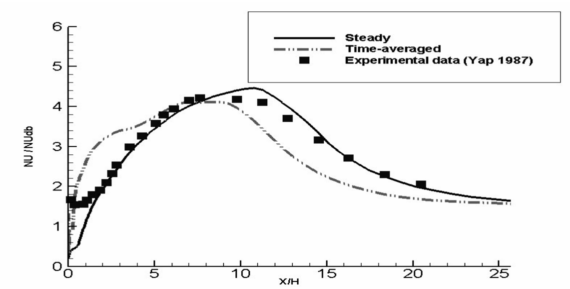

a) Nonlinear $k-\varepsilon$ model

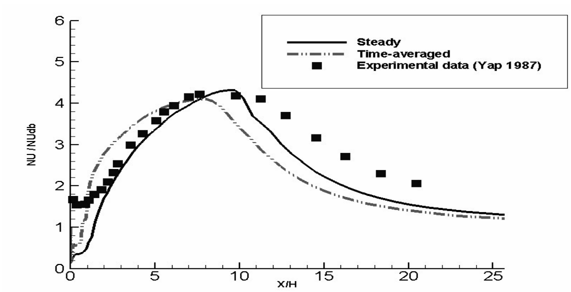

b) Linear $k-\varepsilon$ model

Figure 10 : Nusselt number distribution in the pipe expansion geometry.

CONCLUSIONS

The effects of imposed forcing on flow structures in two kinds of flows with separation and reattachment have been studied numerically. Over a range of forcing frequencies the effect on the time-averaged flow and turbulence levels can be seen in an increase in the turbulence levels in the separated shear layer and a reduction in the size of the separation zone, together with a more intense back flow. As a result the time-averaged heat transfer profiles show higher levels in the separated region, but a peak that is lower and further upstream than in the steady flow case.

Both linear and non-linear $k-\varepsilon$ models have been shown to capture qualitatively the reduction in reattachment length, together with the changes in turbulent and mean velocity profile shapes. The non-linear model generally returns the better quantitative results, including capturing quite accurately the variation of the reattachment length as the forcing frequency is changed.

REFERENCES

Chun, K.B., Sung, H.J., 1996, “Control of turbulent separated flow over a backward-facing step by local forcing”, Experiments in Fluids, Vol. 21, pp. 417-426.

Craft, T.J., Launder, B.E. and Suga, K., 1996, “Development and application of a cubic eddy-viscosity model of turbulence”. Int. J. Heat Fluid Flow, Vol. 17, pp. 108-115.

Craft, T.J., Iacovides, H. and Momeni, P., 2005, “Computations of flow and heat transfer in abrupt pipe expansions using non-linear eddy-viscosity models of turbulence”, Proc. 9th UK National Heat Transfer Conference, Manchester.

Iacovides, H., 1999, “The computation of turbulent flow through stationary and rotating U-bends with rib-roughened surfaces”, Int. J. Numerical Methods in Fluids, Vol. 29, pp. 865-876

Launder, B. E. and Sharma, B.I., 1974, “Application of the energy dissipation model of turbulence to the calculation of flow near a spinning disc”. Lett. Heat Mass Transfer, Vol. 1, pp. 131-138.

Raisee, M., 1999, “Computation of flow and heat transfer through two and three-dimensional rib-roughened passages”. Ph.D. Thesis, UMIST.

Rhie, C. M. and Chow, W. L., 1983, “Numerical study of turbulent flow past an airfoil with trailing edge separation”. *AIAA J.*, Vol. 21, pp. 1525-1532.

Suga, K., 1996, “Development and application of a non-linear eddy-viscosity model sensitised to stress and strain invariants”, PhD. Thesis, Faculty of Technology, University of Manchester.

Yap, C.R., 1987, “Turbulent heat and momentum transfer in recirculating and impinging flows”, PhD. Thesis, Faculty of Technology, University of Manchester.